Macromolecules

ARTICLE

pubs.acs.org/Macromolecules

Macro- and Microphase Separation in Multifunctional Supramolecular Polymer Networks

Zoltan Mester,[†] Aruna Mohan,[†] and Glenn H. Fredrickson*[,†,‡]

[†]Department of Chemical Engineering, University of California, Santa Barbara, California 93106, United States

[‡]Department of Materials and Materials Research Laboratory, University of California, Santa Barbara, California 93106, United States

ABSTRACT: We present a field-based model for the phase separation and gelation of a binary melt of multifunctional monomeric units that can reversibly bond to form copolymer networks. The mean-field phase separation behavior of several model networks with heterogeneous bonding is calculated via the random phase approximation (RPA). By this technique, the spinodal phase boundary (stability limit of the homogeneous disordered phase) is obtained by a combination of analytical and numerical methods. It is demonstrated that higher functionality and more favorable bonding energy suppresses macroscopic phase separation due to greater connectivity between unlike species. Gelation occurs with sufficiently high connectivity of tri- or higher functional monomeric units and microphase separation of the copolymer network can occur either preceding or after the gel point. Eutectic-like behavior of the spinodal is seen in highly connected networks due to excess loosely connected material in systems having nonstoichiometric ratios of the two components.

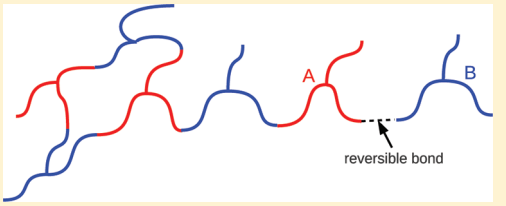

1. INTRODUCTION

In this paper, we explore the phase separation and gelation of a binary melt of reversibly bonded multifunctional polymers. Specifically, we consider a melt blend of star-shaped A and B polymers with r_A and r_B arms, respectively, and functional groups capable of reversible binding at the terminus of each arm. These objects are shown in Figure 1 and because of their propensity to link into larger polymers will be referred to as "monomers" in the present discourse. By virtue of these linkages, monomeric units having functionalities of three or higher can form macroscopic copolymer networks. Gelation occurs when the network reaches the dimensions of the sample itself. In familiar vulcanization, branching occurs via sulfide cross-linkages and gelation proceeds irreversibly.[1] The advantage of thermoreversibly bonded networks over vulcanized rubbers is that the branching that leads to gelation can be controlled via the thermal tuning of connectivity. Moreover, the reversible bonding allows for more varied physical properties and melting and reprocessing of the polymer.

The subject of supramolecular copolymer networks is motivated by the many applications of multifunctional, reversibly bonding polymers, which include block copolymer lithography[2] and multistimuli, multiresponsive metallo-supramolecular polymers.[3] Of particular interest is thermoreversible association via hydrogen bonding, occurring in systems such as ureido-pyrimidone polymer networks described in Lange et al.,[4] supramolecular crystalline networks described in Kihara et al.,[5] and self-healing rubbers described in Chino and Ashiura[6] and Cordier et al.[7] Hydrogen-bonded networks do not experience the thermal degradation of functional groups during reprocessing that is seen in reversibly bonded covalent networks.[4] The self-healing rubbers described in Cordier et al.,[7] consisting of a mixture of difunctional and trifunctional components, can be repaired by bringing fractured surfaces together. These cross-linked networks show extensibility of several hundred percent and little creep under load. Skrzeszewska et al.[8] studied the fracture and healing of self-healing rubbers in the gel phase. The fracture occurs with a delay in time that decreases exponentially with the shear stress, and the gel heals completely after fracture. Sijbesma et al.[9] synthesized di- and trifunctional polymers, which were used to form supramolecular chains and networks. Thermal control over bonding was used to tune viscosity, chain length, and composition.

The theoretical modeling of copolymer networks requires an understanding of their gelation behavior. Flory[1] pioneered the theory of gelation for polyfunctional condensation of a homogeneous material through probabilistic and combinatorial arguments. The condition for gelation can be expressed in terms of the fraction of functional groups reacted, denoted by α. For r functional branching units, the weight-average molecular weight of the copolymer network diverges at the critical fractional conversion $\alpha_c = 1/(r - 1)$. This result was independently obtained by Stockmayer.[10] Coniglio et al.[11,12] derived a statistical mechanical model that, unlike the bond percolation problem in the Flory–Stockmayer model, incorporates solvent molecules and interactions between molecules, and obtained a closed form solution for the Bethe lattice. This work predicts the termination of the gel–sol phase boundary curve at the critical solution point of the monomer–solvent binary coexistence curve under certain

Received: July 10, 2011
Revised: October 17, 2011
Published: November 15, 2011

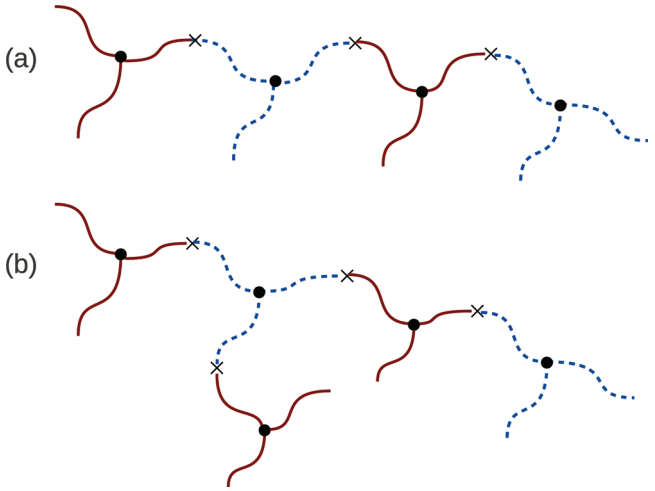

Figure 1. Schematic illustration of (a) linear and (b) branched clusters with $r_A = r_B = 3$ for A and B type monomeric units. The circles represent nodes and the crosses represent reacted terminals. The arms of the A type monomeric units are red, solid curves and the arms of the B type monomeric units are blue, dashed curves. Reaction is only permitted between unlike monomeric unit arm ends.

conditions and the existence of a maximum temperature above which gelation does not occur. Prior studies have also considered the dynamics of the formation of persistent structures and dynamic heterogeneities.[13−16] Here, however, we focus exclusively on the equilibrium state; a phase is defined to be a "gel" if its weight-average molecular weight is macroscopic. The mechanical and rheological characteristics of such a gel phase evidently depend on the lifetimes of its persistent structures compared to the rate and history of deformation.

Gordon and co-workers[17−25] provided a sound statistical mechanical basis for Flory−Stockmayer theory by deriving the condition for gelation via statistical mechanics and graph theory. This work relies on the relation of the reaction equilibria to the symmetries of the reactants and products, where the latter are quantified via the enumeration of trees from a graphical representation of the polymers. Nonetheless, the theory is restricted to spatially homogeneous networks and is therefore not suitable for addressing questions of macro- and microphase separation that may take place either prior to or after gelation.

Mohan et al.[26] presented a methodology for a single component *inhomogeneous* network by embedding the formalism of Gordon and co-workers into a field-theoretic model of continuous Gaussian chains, thereby quantifying the spatially dependent conformational entropies of all isomeric chain configurations. It was shown that Flory−Stockmayer theory is recovered in the homogeneous limit, and the formalism was applied to describe gelation under confinement in a good solvent as an illustration of an inhomogeneous system. Furthermore, the formalism of Mohan et al. is capable of describing the pregelation and postgelation regimes in inhomogeneous networks.

Here, we extend the model of Mohan et al. to describe the phase behavior and gelation of a binary melt of r_A-armed A monomeric units with polymerization N_A for each arm and r_B-armed B monomeric units with polymerization N_B for each arm, and with functional ends at each arm (Figure 1). Previous theoretical studies exploring the phase behavior of AB type block copolymers have been limited primarily to linear architectures, or small well-defined branched architectures, such as A_nB_n miktopolymers or $(AB)_n$ radial copolymers. Linear copolymers[27−29] show a variety of ordered microstructures that minimize energetically unfavorable interactions between unlike blocks while maximizing chain conformational entropy. Furthermore, the presence of homopolymer in a block copolymer composition can lead to macrophase separation.[30−32] Considerably less theoretical work has been conducted on reversibly bonding copolymer systems using either numerical self-consistent field theory, or the simplified random phase approximation (RPA). Recent examples of such studies include supramolecular diblock melts,[33] supramolecular triblock melts,[34] and binary melts of difunctional polymers.[35]

The present work explores the spinodal phase boundaries between the homogeneous disordered phase and A-rich and B-rich coexisting homogeneous phases or ordered microphases for a binary melt of multifunctional monomeric units, and identifies the gelation point along these boundaries. Section 2 presents the field-theoretic model and the RPA formalism. The details of the derivations are relegated to the Appendices. Section 3 presents the results of these studies including phase boundaries and weight-average molecular weights as a function of the fraction of functional groups reacted. Section 4 summarizes these results and discusses a variety of extensions of our work.

2. THEORETICAL METHODS

2.1. Field-Theoretic Model. We consider a melt blend of star-shaped multifunctional polymers consisting of n_A A monomeric units, each having r_A arms, and n_B B monomeric units, each having r_B arms, which can reversibly bond at the functional ends of the arms. The chain statistics of the A arms of polymerization index N_A and B arms of polymerization index N_B are described by the continuous Gaussian chain model. The grand canonical ensemble is used to incorporate the reaction equilibria between A and B functional ends into the model and determine the connectivity of the network. A particle-to-field transformation is subsequently invoked to create a statistical field theory model of the interacting network blend.

The grand canonical partition function with the particle−particle interactions decoupled via position-dependent pressure (+) and exchange (−) potential fields $w_\pm(\mathbf{r})$, where $\mathbf{r}$ denotes position, is given by the expression[36]

$$Z_G(\{z_{n_A,n_B,k}\},V,T) = Z_0 \int \mathcal{D}w_+ \int \mathcal{D}w_- \exp(-H_G[w_\pm]) \tag{1}$$

where Z_0 is the ideal gas partition function of the polymer and $\{z_{n_An_Bk}\}$ is the set of activities involving all possible isomers (indexed by k) of clusters with any number n_A A monomeric units and n_B B monomeric units. V denotes the volume of the system, and T is temperature. The Hamiltonian H_G in units of k_BT, where k_B is Boltzmann's constant, is written as[36]

$$H_G[w_\pm] = \rho_0 \int \mathrm{d}\mathbf{r}\,[(1/\chi)w_-^2 - iw_+] - \sum_{n_A,n_B=0}^{\infty} \sum_k z_{n_A,n_B,k} V Q_{n_A,n_B,k}[w_\pm] \tag{2}$$

where $Q_{n_An_Bk}[w_\pm]$ is the single chain partition function of the kth isomer of a cluster containing n_A A monomers and n_B B monomers

and ρ_0 is the total monomer density of the sample, which is assumed to be uniform (incompressible liquid assumption).

The activity of a cluster in its kth isomeric form composed of n_A A monomeric units and n_B B monomeric units, $z_{n_A n_B k}$ is related to the activities of the individual A monomeric units and B monomeric units, z_A and z_B, respectively, through reaction equilibria and the law of mass action via the relation

$$\frac{z_{n_A,n_B,k}}{z_A^{n_A} z_B^{n_B}} = \frac{1}{\rho_0^{n_A+n_B-1}} e^{-\Delta G_{n_A,n_B,k}/k_B T} \tag{3}$$

where $\Delta G_{n_A n_B k}$ is the free energy of formation of the kth isomer of the cluster with n_A A monomeric units and n_B B monomeric units. The free energy of formation may be expressed in the form

$$\Delta G_{n_A,n_B,k} = \Delta G^0_{AA} l_{AA} + \Delta G^0_{BB} l_{BB} + \Delta G^0_{AB} l_{AB} - T\Delta S_{comb,n_A,n_B,k} \tag{4}$$

where ΔG^0_{AA}, ΔG^0_{BB}, ΔG^0_{AB} are the fundamental free energies of formation for a single A−A, B−B, and A−B bond, respectively, l_{AA}, l_{BB}, and l_{AB} are the number of A−A, B−B, and A−B bonds, respectively, and $\Delta S_{comb,n_A n_B k}$ is the combinatorial entropy of formation of the kth isomer of a cluster with n_A A monomeric units and n_B B monomeric units.[17−20,37]

The ratio of activities in eq 3, i.e., the equilibrium constant, can be expressed as a ratio of the partition functions of its products and reactants.[37] The partition functions may be decomposed into a product of contributions from translational, rotational, vibrational, electronic and nuclear modes.[37] The contribution to the free energy of formation from the combinatorial entropy change, $\Delta S_{comb,n_A n_B k}$, contains the contribution from the inverse dependence of the rotational partition functions on their symmetry numbers, while the remaining energetic and entropic contributions are contained in the term $\Delta G^0_{AA} l_{AA} + \Delta G^0_{BB} l_{BB} + \Delta G^0_{AB} l_{AB}$.[17−20,37] The combinatorial entropy of formation is defined by the expression[17−20]

$$\Delta S_{comb,n_A,n_B,k} = k_B \ln\left(\frac{|G_A|^{n_A}|G_B|^{n_B}}{|G_{n_A,n_B,k}|}\right) \tag{5}$$

where $|G_A| = r_A!$ and $|G_B| = r_B!$ are the symmetry numbers of single A and B monomeric units, respectively, assumed to be symmetric to all permutations of the arms. The symmetry number of the cluster, denoted by $|G_{n_A n_B k}|$, is related to the number of distinct rooted, ordered trees[38,39] obtained from the graph of the polymer cluster.[17−20] This relationship enables the simplification of eq 3 and, consequently, eq 2. We present the final results below, while the details are relegated to Appendix A.

The summations in the Hamiltonian in eq 2 are achieved via the introduction of generating functions[20,38] F_{0A} and F_{0B} for tree configurations. The final form of the Hamiltonian is

$$H_G[w_\pm] = \rho_0 \int d\mathbf{r}\,[(1/\chi)w_-^2 - iw_+] - z_A \int d\mathbf{r} \int_0^1 d\theta_A\, F_{0A}(\mathbf{r},\theta_A,\theta_B = 1,[w_\pm]) - z_B \int d\mathbf{r} \int_0^1 d\theta\, {}_B F_{0B}(\mathbf{r},\theta_A = 0,\theta_B,[w_\pm]) \tag{6}$$

or, equivalently

$$H_G[w_\pm] = \rho_0 \int d\mathbf{r}\,[(1/\chi)w_-^2 - iw_+] - z_B \int d\mathbf{r} \int_0^1 d\theta_B F_{0B}(\mathbf{r},\theta_A = 1,\theta_B,[w_\pm]) - z_A \int d\mathbf{r} \int_0^1 d\theta_A\, F_{0A}(\mathbf{r},\theta_A,\theta_B = 0,[w_\pm]) \tag{7}$$

The generating functions F_{0A} and F_{0B} are defined recursively by the following equations:

$$F_{0A} = \left(q_{0A}(N_A) + \frac{z_B r_B}{\rho_0} e^{-\Delta G^0_{AB}/k_B T}\theta_B G_{A,N_A} * G_{B,N_B} * F_{1B} + \frac{z_A r_A}{\rho_0} e^{-\Delta G^0_{AA}/k_B T}\theta_A G_{A,2N_A} * F_{1A}\right)^{r_A} \tag{8}$$

and

$$F_{0B} = \left(q_{0B}(N_B) + \frac{z_A r_A}{\rho_0} e^{-\Delta G^0_{AB}/k_B T}\theta_A G_{B,N_B} * G_{A,N_A} * F_{1A} + \frac{z_B r_B}{\rho_0} e^{-\Delta G^0_{BB}/k_B T}\theta_B G_{B,2N_B} * F_{1B}\right)^{r_B} \tag{9}$$

with

$$F_{1A} = \left(q_{0A}(N_A) + \frac{z_B r_B}{\rho_0} e^{-\Delta G^0_{AB}/k_B T}\theta_B G_{A,N_A} * G_{B,N_B} * F_{1B} + \frac{z_A r_A}{\rho_0} e^{-\Delta G^0_{AA}/k_B T}\theta_A G_{A,2N_A} * F_{1A}\right)^{r_A - 1} \tag{10}$$

and

$$F_{1B} = \left(q_{0B}(N_B) + \frac{z_A r_A}{\rho_0} e^{-\Delta G^0_{AB}/k_B T}\theta_A G_{B,N_B} * G_{A,N_A} * F_{1A} + \frac{z_B r_B}{\rho_0} e^{-\Delta G^0_{BB}/k_B T}\theta_B G_{B,2N_B} * F_{1B}\right)^{r_B - 1} \tag{11}$$

where $q_{0A}(s) = q_0(\mathbf{r},s,[w_A])$ and $q_{0B}(s) = q_0(\mathbf{r},s,[w_B])$ denote chain end propagators for A and B chain arms starting from a free chain end, with the field $w_A = iw_+ - w_-$ acting on A segments and the field $w_B = iw_+ + w_-$ acting on B segments. The convolution operator "$*$" denotes the following:

$$G_{J,s} * g = \int d\mathbf{r}'\, G(\mathbf{r},\mathbf{r}',s,[w_J])g(\mathbf{r}') \tag{12}$$

for any arbitrary function g, where $J = \{A,B\}$ and s denotes a position along the chain contour. The chain end propagator in the field w_J is

$$q_0(\mathbf{r},s,[w_J]) = \int d\mathbf{r}'\, G(\mathbf{r},\mathbf{r}',s,[w_J]) \tag{13}$$

where the function $G(\mathbf{r},\mathbf{r}',s,[w_J])$ is the Green's function for diffusion in the field w_J. The Green's function satisfies

$$\frac{\partial G(\mathbf{r},\mathbf{r}',s;[w_J])}{\partial s} = \frac{b^2}{6}\nabla^2_{\mathbf{r}} G(\mathbf{r},\mathbf{r}',s;[w_J]) - w_J(\mathbf{r})G(\mathbf{r},\mathbf{r}',s;[w_J]) \tag{14}$$

with the initial condition $G(\mathbf{r},\mathbf{r}',0;[w_i]) = \delta(\mathbf{r}-\mathbf{r}')$. The parameter b is the statistical segment length of the polymer, which is assumed to be the same for both A and B components.

The functions F_{0A} and F_{0B} in eq 8 and eq 9 represent generating functions for rooted, ordered trees rooted on A units, with r_A edges emanating from the root node, and rooted on B units, with r_B edges emanating from the root node, respectively. Similarly, F_{1A} and F_{1B} denote generating functions for subtrees rooted on A units and B units, respectively, with $r_A - 1$ and $r_B - 1$ edges, respectively, emanating from the root nodes of the corresponding subtrees. The variables θ_A and θ_B are auxiliary variables, such that the coefficient of $\theta_A^{n_A-1}\theta_B^{n_B}$ in the expansion of F_{0A} represents trees having n_A A-nodes and n_B B-nodes rooted on an A-node. Similarly, the coefficient of $\theta_A^{n_A}\theta_B^{n_B-1}$ in the expansion of F_{0B} represents trees having n_A A-nodes and n_B B-nodes rooted on a B-node. The three terms appearing within parentheses on the right-hand side of eq 8 and eq 10 denote an unreacted arm of the root A unit, an arm bonded to a B unit and an arm bonded to another A unit, respectively. The exponent r_A appearing on the right-hand side of eq 8 arises from the presence of r_A arms emanating from the root A unit of the tree, whereas the exponent $r_A - 1$ in eq 10 denotes the $r_A - 1$ edges corresponding to the root A node of a subtree. The generating functions F_{0B} and F_{1B} for trees and subtrees rooted at B nodes, having r_B and $r_B - 1$ edges corresponding to the root node, respectively, are similarly constructed, and the terms within parentheses on the right-hand side of eq 9 and eq 11 denote an unreacted arm of a root B unit, an arm bonded to an A unit and an arm bonded to another B unit, respectively. The pregelation and postgelation regimes are described by appropriately selecting the roots of F_{1A} and F_{1B}, as described in Appendix A.

The segment densities, $\rho_A(\mathbf{r};[w_\pm])$ and $\rho_B(\mathbf{r};[w_\pm])$, for the A and B component segments, respectively, are given by

$$\rho_A(\mathbf{r};[w_\pm]) = -\sum_{n_A,n_B=0}^{\infty}\sum_k z_{n_A,n_B,k}V\frac{\delta Q_{n_A,n_B,k}[w_\pm]}{\delta[w_A(\mathbf{r})]} \quad (15)$$

and

$$\rho_B(\mathbf{r};[w_\pm]) = -\sum_{n_A,n_B=0}^{\infty}\sum_k z_{n_A,n_B,k}V\frac{\delta Q_{n_A,n_B,k}[w_\pm]}{\delta[w_B(\mathbf{r})]} \quad (16)$$

The densities in eq 15 and eq 16 may be simplified by applying the factorization property of the partition function[36] and by computing the contribution from each arm of every polymer chain in the system. Consequently, the segment densities can be expressed in terms of the generating functions F_{1A} and F_{1B} as follows:

$$\rho_A(\mathbf{r}) = z_A r_A\int_0^{N_A} ds\,\{(G_{A,N_A-s} * F_{1A}) \times\left[G_{A,s} * \left(1 + \frac{z_A r_A}{\rho_0}e^{-\Delta G^0_{AA}/k_BT}G_{A,N_A} * F_{1A} + \frac{z_B r_B}{\rho_0}e^{-\Delta G^0_{AB}/k_BT}G_{B,N_B} * F_{1B}\right)\right]\}_{\theta_A=\theta_B=1} \quad (17)$$

and

$$\rho_B(\mathbf{r}) = z_B r_B\int_0^{N_B} ds\,\{(G_{B,N_B-s} * F_{1B}) \times\left[G_{B,s} * \left(1 + \frac{z_A r_A}{\rho_0}e^{-\Delta G^0_{AB}/k_BT}G_{A,N_A} * F_{1A} + \frac{z_B r_B}{\rho_0}e^{-\Delta G^0_{BB}/k_BT}G_{B,N_B} * F_{1B}\right)\right]\}_{\theta_A=\theta_B=1} \quad (18)$$

The first term within parentheses on the right-hand side of eq 17 represents the statistical weight of a segment on an arm of an A unit, at a contour distance of $N_A - s$ measured along the arm from the junction of the arms, and the second term represents the statistical weight of the same segment at a contour distance s measured from the arm end, where the arm end may be unreacted, bonded to another A unit or bonded to a B unit. Integration over the contour position s yields the segment density ρ_A at $\mathbf{r}$. The factor r_A arises in eq 17 and the integral over θ_A appearing in eq 6 is eliminated due to the presence of $r_A n_A$ A-arms in total. The segment density ρ_B of B units, given by eq 18, is constructed analogously.

The end segment densities are obtained by omitting the integral over s and setting $s = 0$ in eq 17 and eq 18, corresponding to end points of A and B arms, respectively. The end segment densities are given by

$$\rho_{A,e}(\mathbf{r}) = z_A r_A(G_{A,N_A} * F_{1A}) \times\left[1 + \frac{z_A r_A}{\rho_0}e^{-\Delta G^0_{AA}/k_BT}G_{A,N_A} * F_{1A} + \frac{z_B r_B}{\rho_0}e^{-\Delta G^0_{AB}/k_BT}G_{B,N_B} * F_{1B}\right]_{\theta_A=\theta_B=1} \quad (19)$$

and

$$\rho_{B,e}(\mathbf{r}) = z_B r_B(G_{B,N_B} * F_{1B}) \times\left[1 + \frac{z_A r_A}{\rho_0}e^{-\Delta G^0_{AB}/k_BT}G_{A,N_A} * F_{1A} + \frac{z_B r_B}{\rho_0}e^{-\Delta G^0_{BB}/k_BT}G_{B,N_B} * F_{1B}\right]_{\theta_A=\theta_B=1} \quad (20)$$

The unreacted end segment densities are obtained from eq 19 and eq 20 by retaining only the contribution arising from unreacted terminals. These expressions have the form

$$\rho_{A,ue}(\mathbf{r}) = z_A r_A(G_{A,N_A} * F_{1A})_{\theta_A=\theta_B=1} \quad (21)$$

$$\rho_{B,ue}(\mathbf{r}) = z_B r_B(G_{B,N_B} * F_{1B})_{\theta_A=\theta_B=1} \quad (22)$$

The fractions of reacted A and B functional ends are given, respectively, by

$$\alpha_A(\mathbf{r}) = 1 - \frac{\rho_{A,ue}(\mathbf{r})}{\rho_{A,e}(\mathbf{r})} \quad (23)$$

and

$$\alpha_B(\mathbf{r}) = 1 - \frac{\rho_{B,ue}(\mathbf{r})}{\rho_{B,e}(\mathbf{r})} \quad (24)$$

While the above formalism is valid generally, the current work is restricted to the mean-field approximation, made by finding the saddle point of the Hamiltonian in eq 2. The resulting mean-field equations are

$$\left.\frac{\delta H[w_\pm]}{\delta w_-(\mathbf{r})}\right|_{w_\pm=w_\pm^*} = 0 = (2\rho_0/\chi)w_-^*(\mathbf{r}) - \rho_A(\mathbf{r};[w_\pm^*]) + \rho_B(\mathbf{r};[w_\pm^*]) \quad (25)$$

$$\left.\frac{\delta H[w_\pm]}{\delta[iw_+(\mathbf{r})]}\right|_{w_\pm=w_\pm^*} = 0 = -\rho_0 + \rho_A(\mathbf{r};[w_\pm^*]) + \rho_B(\mathbf{r};[w_\pm^*]) \quad (26)$$

where $w_\pm^*$ are the mean-field values of the fields.

The probability $p_{n_A n_B}$ for finding a cluster of n_A A monomeric units and n_B B monomeric units is given by $p_{n_A n_B} \sim \Sigma_k z_{n_A n_B k} V Q_{n_A n_B k}$ to within a normalization factor in the saddle point approximation. Consequently, the weight-average degree of polymerization is given by the equation

$$N_w = \frac{\sum_{n_A, n_B = 0}^{\infty} \sum_k (n_A + n_B)^2 z_{n_A, n_B, k} Q_{n_A, n_B, k}}{\sum_{n_A, n_B = 0}^{\infty} \sum_k (n_A + n_B) z_{n_A, n_B, k} Q_{n_A, n_B, k}}$$

$$= \frac{z_A \int \mathbf{dr} \left.\frac{\partial F_{0A}}{\partial \theta_A}\right|_{\theta_A = 1, \theta_B = 1} + z_B \int \mathbf{dr} \left.\frac{\partial F_{0B}}{\partial \theta_B}\right|_{\theta_A = 1, \theta_B = 1} + 2 z_A \int \mathbf{dr} \left.\frac{\partial F_{0A}}{\partial \theta_B}\right|_{\theta_A = 1, \theta_B = 1}}{z_A \int \mathbf{dr}\, F_{0A}|_{\theta_A = 1, \theta_B = 1} + z_B \int \mathbf{dr}\, F_{0B}|_{\theta_A = 1, \theta_B = 1}} + 1 \quad (27)$$

where our definition of the weight-average degree of polymerization does not include the relative mass weightings of N_A and N_B. Gelation occurs when the weight-average degree of polymerization diverges, $N_w \rightarrow \infty$.

For convenience, the following scaled variables are introduced:

$$\bar{\mathbf{r}} = \frac{\mathbf{r}}{R_g}, \quad \bar{V} = \frac{V}{{R_g}^3}, \quad \phi_J = \frac{\rho_J}{\rho_0},$$

$$\bar{z}_J = \frac{z_J N_A}{\rho_0}, \quad \bar{z}_{n_A, n_B, k} = z_{n_A, n_B, k} \frac{N_A}{\rho_0}, \quad \bar{s} = \frac{s}{N_A}, \quad \bar{w}_J = w_J N_A \quad (28)$$

where the radius of gyration R_g is given by ${R_g}^2 = b^2 N_A/6$. Furthermore, in this paper we will consider only the limit of heterogeneous bonding, with $\Delta G^0_{AA} \rightarrow \infty$ and $\Delta G^0_{BB} \rightarrow \infty$.

When re-expressed in terms of the above scaled variables in the heterogeneous bonding limit, eq 17 and eq 18 yield the following expressions for the volume fractions ϕ_A and ϕ_B for the A and B species, respectively:

$$\phi_A(\bar{\mathbf{r}}) = \bar{z}_A r_A \int_0^1 \mathrm{d}\bar{s} \left\{ (G_{A, 1-\bar{s}} * F_{1A}) \times \left[G_{A,\bar{s}} * \left(1 + \frac{\bar{z}_B r_B}{N_A} \mathrm{e}^{-\Delta G^0_{AB}/k_B T} G_{B, \bar{s} = f_B} * F_{1B} \right) \right] \right\}_{\theta_A = \theta_B = 1} \quad (29)$$

and

$$\phi_B(\bar{\mathbf{r}}) = \bar{z}_B r_B \int_0^{f_B} \mathrm{d}\bar{s} \left\{ (G_{B, f_B - \bar{s}} * F_{1B}) \times \left[G_{B,\bar{s}} * \left(1 + \frac{\bar{z}_A r_A}{N_A} \mathrm{e}^{-\Delta G^0_{AB}/k_B T} G_{A, \bar{s}=1} * F_{1A} \right) \right] \right\}_{\theta_A = \theta_B = 1} \quad (30)$$

where the scaled length of the B arms f_B is given by $f_B = N_B/N_A$. The generating functions F_{1A} and F_{1B} given by eq 10 and eq 11 further reduce in the heterogeneous bonding limit to

$$F_{1A} = \left(q_{0A}(\bar{s} = 1) + \frac{\bar{z}_B r_B}{N_A} \mathrm{e}^{-\Delta G^0_{AB}/k_B T} \theta_B G_{A, \bar{s}=1} G_{B, \bar{s}=f_B} * F_{1B} \right)^{r_A - 1} \quad (31)$$

and

$$F_{1B} = \left(q_{0B}(\bar{s} = f_B) + \frac{\bar{z}_A r_A}{N_A} \mathrm{e}^{-\Delta G^0_{AB}/k_B T} \theta_A G_{B, \bar{s}=f_B} * G_{A, \bar{s}=1} * F_{1A} \right)^{r_B - 1} \quad (32)$$

Inspection of eqs 29−32 reveals that the strength of bonding reactions is characterized by the parameter $\mathrm{e}^{-\Delta G^0_{AB}/(k_B T)}/N_A$. Therefore, we define an effective bonding energy $h_{\mathrm{eff}} = -\Delta G^0_{AB}/(k_B T) - \ln(N_A)$.

The mean-field equations reduce to the following:

$$\frac{1}{\chi N_A} \bar{w}_-{}^*(\bar{\mathbf{r}}) - \phi_A(\bar{\mathbf{r}}; [\bar{w}_\pm{}^*]) + \phi_B(\bar{\mathbf{r}}; [\bar{w}_\pm{}^*]) = 0 \quad (33)$$

and

$$-1 + \phi_A(\bar{\mathbf{r}}; [\bar{w}_\pm{}^*]) + \phi_B(\bar{\mathbf{r}}; [\bar{w}_\pm{}^*]) = 0 \quad (34)$$

where the latter equation evidently imposes the incompressibility constraint.

For spatially homogeneous systems, the gelation condition is given by

$$\alpha_{A,c} = \sqrt{\frac{\phi_B N_A}{\phi_A N_B (r_A - 1)(r_B - 1)}} \quad (35)$$

and

$$\alpha_{B,c} = \sqrt{\frac{\phi_A N_B}{\phi_B N_A (r_A - 1)(r_B - 1)}} \quad (36)$$

where the subscript "c" refers to the critical fractional conversions at the gel point. The gelation condition given by equations eq 35 and eq 36 applies in the heterogeneous bonding limit since the derivation makes use of

$$\frac{\alpha_A}{\alpha_B} = \frac{N_A \phi_B}{N_B \phi_A} \quad (37)$$

which results from A and B monomeric units having the same number of reacted end segments. In the more general case where homogeneous bonding can occur between two A units or between two B units, in addition to heterogeneous bonding between A and B units, three parameters are required to identify the numbers of A−A, A−B and B−B bonds, and α_A and α_B alone are insufficient to fully characterize the generating functions. The derivation of the gelation condition is described in Appendix C.

The present formalism is suitable for both homogeneous and inhomogeneous phases. The current work explores the homogeneous phase and, via a weak inhomogeneity expansion (the so-called random phase approximation), the stability limit of the homogeneous phase. This dramatically simplifies the equations by making the fields and volume fractions spatially independent. Owing to the incompressibility constraint, only one of the two monomer activities proves to be independent; hence, z_A was set to a constant in our numerical solutions. The binodals for coexistence of two homogeneous phases are numerically calculated by selecting the value of z_B that results in two phases with equal mean-field Hamiltonians and, hence, equal osmotic pressures in the grand canonical ensemble. The mean-field equations given by eq 33 and eq 34 are solved by continuous steepest descent and ascent schemes.[38] The $F_{1A}^{(0)}$ and $F_{1B}^{(0)}$ spatially homogeneous generating functions are obtained from eq 72 and eq 73 using the Newton−Raphson method.[40]

2.2. Random Phase Approximation. The spinodal or stability limit of the melt is found by applying the random phase approximation (RPA). We consider weak spatially varying field perturbations of the form

$$\overline{w}_J(\vec{\mathbf{r}}) = \overline{w}_{J,0} + \varepsilon\omega_J(\vec{\mathbf{r}}) \tag{38}$$

where $\overline{w}_{J,0}$ is the mean value of the field given by

$$\overline{w}_{J,0} = \frac{1}{\overline{V}}\int \mathrm{d}\vec{\mathbf{r}}\, \overline{w}_J(\vec{\mathbf{r}}) \tag{39}$$

ε is a positive constant such that $\varepsilon \ll 1$ and $\omega_J(\vec{\mathbf{r}})$ is the spatially varying part of the field. Upon substitution of eq 38 in eq 29 and eq 30, and expanding the necessary generating functions to the first order in ε, the volume fractions may be expressed in the form

$$\phi_J(\vec{\mathbf{r}}) = \phi_J^{(0)} + \delta\phi_J(\vec{\mathbf{r}}) \tag{40}$$

where $\phi_J^{(0)}$ are the $\mathcal{O}(1)$ and $\delta\phi_J(\vec{\mathbf{r}})$ are the $\mathcal{O}(\varepsilon)$ terms of the expansion. The details of this expansion procedure are contained in Appendix B.

The $\delta\phi_J(\vec{\mathbf{r}})$ terms can be expressed in Fourier space in the form

$$\delta\phi_A(\vec{\mathbf{k}}) = S_{AA}(\vec{\mathbf{k}})\omega_A(\vec{\mathbf{k}}) + S_{AB}(\vec{\mathbf{k}})\omega_B(\vec{\mathbf{k}}) \tag{41}$$

$$\delta\phi_B(\vec{\mathbf{k}}) = S_{AB}(\vec{\mathbf{k}})\omega_A(\vec{\mathbf{k}}) + S_{BB}(\vec{\mathbf{k}})\omega_B(\vec{\mathbf{k}}) \tag{42}$$

whereby we obtain the density−density correlation functions (structure factors) in Fourier space for Gaussian clusters in the absence of external fields, $S_{AA}(\overline{k})$, $S_{AB}(\overline{k})$ and $S_{BB}(\overline{k})$, where $\overline{k}$ is the dimensionless wavenumber, made dimensionless with the scale R_g, and related to dimensionless the wave vector $\vec{\mathbf{k}}$ via the definition $\overline{k} = |\vec{\mathbf{k}}|$.

The correlation functions obtained from eq 41 and eq 42 are used to calculate the limit of stability from the inverse scattering function given by the expression[27]

$$S^{-1}(\overline{k}) = \frac{S_{AA}(\overline{k}) + 2S_{AB}(\overline{k}) + S_{BB}(\overline{k})}{S_{AA}(\overline{k})S_{BB}(\overline{k}) - S_{AB}{}^2(\overline{k})} - 2\chi N_A \tag{43}$$

The limit of stability is indicated by a divergence in the scattering function, $S(\overline{k}^*)\rightarrow\infty$, at a critical value of the wavenumber, $\overline{k} = \overline{k}^*$. If the scattering function diverges at a finite value of $\overline{k}^*$, a periodic phase of periodicity $2\pi/\overline{k}^*$ (i.e., microphase) forms upon crossing the spinodal. In contrast, if $S(\overline{k})$ diverges at $\overline{k} = 0$, then the homogeneous phase is unstable against macrophase separation into two homogeneous phases. The spinodal is thus found by computing the zeros of the inverse scattering function, $S^{-1}(\overline{k}) = 0$, at its minimum with respect to $\overline{k}$, while simultaneously satisfying the spatially homogeneous mean-field equations. As before, z_A is set to a constant, and z_B is selected to yield a specified volume fraction. Equation 72 and eq 73 are also solved to obtain $F_{1A}^{(0)}$ and $F_{1B}^{(0)}$. The solutions to the above equations are obtained with the Newton−Raphson method.[40]

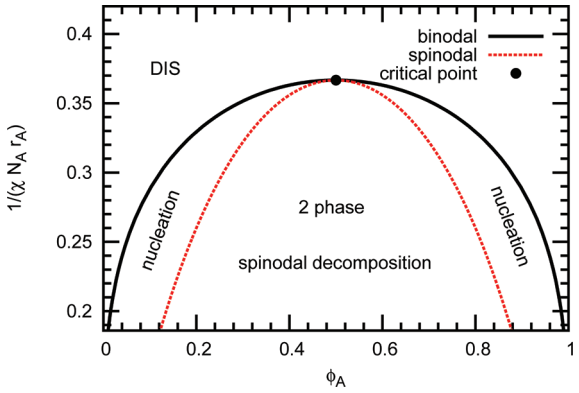

Figure 2. Mean-field phase diagram in coordinates of $(\chi N_A r_A)^{-1}$ versus ϕ_A for bond strength of $h_{eff} = 1 - \ln 10$ and $r_A = r_B = 3$ arm A and B type monomeric units. Labeled phases are DIS (homogeneous disordered) and 2 phase (coexisting A-rich and B-rich homogeneous phases). The phase separation between the binodal and spinodal occurs via nucleation, and, within the spinodal, it takes place spontaneously via spinodal decomposition.

3. RESULTS

Here we examine the stability of a spatially homogeneous system of heterogeneously bonded A and B monomeric units of functionalities r_A and r_B, respectively, with effective bonding energy $h_{eff} = -\Delta G_{AB}^0/(k_BT) - \ln(N_A)$ and equal degrees of polymerization $N_A = N_B$ of the arms. The spinodals, binodals, and weight-average molecular weight are calculated numerically by applying the methods described in section 2 and the Appendix.

The phase behavior of a symmetric system consisting of $r_A = r_B$ A and B arm monomeric units is first considered. Figure 2 depicts the binodal and spinodal in coordinates of $(\chi N_A r_A)^{-1}$ (a temperature-like variable since $\chi \sim 1/T$) versus ϕ_A for networks with $h_{eff} = 1 - \ln 10$ and functionalities $r_A = r_B = 3$. Values of $-(\Delta G_{AB}^0)/(k_BT) = 1$ and $N_A = N_B = 10$ are chosen for convenience, but this and subsequent plots apply to all combinations of $(\Delta G_{AB}^0)/(k_BT)$ and $N_A = N_B$ that yield the proper value of h_{eff}. Inside the phase envelope, indicated by the binodal, the sample separates into A-rich and B-rich homogeneous phases. The phase separation between the binodal and spinodal occurs via nucleation, and, within the spinodal, it takes place spontaneously via spinodal decomposition.

Figure 3 depicts the spinodal in coordinates of $(\chi N_A r_A)^{-1}$ versus ϕ_A for the same polymer system as in Figure 2, but with $h_{eff} = 7 - \ln 10$. Above the values of $(\chi N_A r_A)^{-1}$ indicated by the Lifshitz points, the spinodal corresponds to the limit of stability with microphases with wave numbers $k^* > 0$. Below these Lifshitz point values, it corresponds to the limit of stability with coexisting homogeneous macrophases with wavenumber $k^* = 0$. The envelope denoted by the spinodal encloses a region where phase separation takes place via spinodal decomposition. At $\phi_A = 0.5$

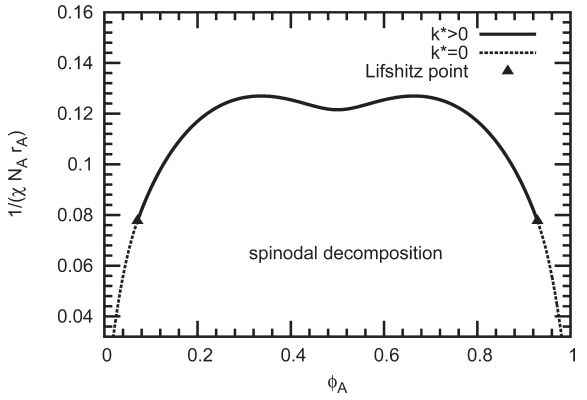

Figure 3. The limit of stability in coordinates of $(\chi N_A r_A)^{-1}$ vs ϕ_A with coexisting A-rich and B-rich homogeneous phases, wavenumber $k^* = 0$, and microphases, wavenumber $k^* > 0$, with bond strength $h_{eff} = 7 - \ln 10$ for $r_A = r_B = 3$ arm A and B type monomeric units. The envelope denoted by the spinodal encloses a region where phase separation takes place via spinodal decomposition. The compositions corresponding to the maxima in the curve are referred to as "compounds" and the local minimum at $\phi_A = 0.5$ is the "eutectic point.".

there is a local minimum in the spinodal, which will be referred to as a "eutectic point." The two maxima in the spinodal, which could be identified as "compounds" in a metallurgy context, occur at $\phi_A = 0.336$ and $\phi_A = 0.664$.

Figure 3 indicates the occurrence of compositions in non-stoichiometric ratios with lower miscibility than the composition found at the eutectic point. Miscibility is lower for these non-stoichiometric compositions because the unreacted functional ends of the excess reactant alongside an otherwise highly connected network aids in phase separation. The phase envelope is symmetric with respect to the $\phi_A = 0.5$ axis, since A and B monomeric units have the same number of arms and arm lengths.

Figure 4a shows the compound and eutectic temperatures in the spinodal of $r_A = r_B = 3$ arm A and B monomeric units as a function of h_{eff}. The onset of eutectic-like behavior is seen at the bonding energy $h_{eff} = 2.683$. The compound and eutectic compositions in terms of volume fractions are illustrated by Figure 4b. The increased separation of the branches corresponding to the compounds and eutectic points in terms of both ϕ_A and $\chi N_A r_A$ with increased bond strength h_{eff} results from the greater difficulty of microphase separation in copolymer networks with higher connectivity that results from having functional ends in stoichiometric ratios.

Figure 5 shows the mean-field phase diagram of a system consisting of $r_A = r_B = 3$ arm A and B monomeric units on the $z_A/z_B = 1$ isopleth in $(\chi N_A r_A)^{-1}$ versus h_{eff} coordinates. The isopleth corresponds to a composition of $\phi_A = 0.5$ in the homogeneous disordered phase. The binodal separating gel and nongel homogeneous disordered and phase separated regions is obtained from calculating the spinodal along the critical points on the isopleth. The binodal indicates that the phase boundary separating the disordered region from the homogeneous coexisting 2 phase region tends toward the value given by Flory–Huggins theory for the nonbonding system, $(\chi N_A r_A)^{-1} = 0.5$, as $h_{eff} \rightarrow -\infty$. When eutectic behavior appears, the isopleth spinodal may not be identical to the binodal and is treated as an approximation to the binodal, which is indicated by a dashed curve. The curves with double hatch marks and alternating dash and hatch marks

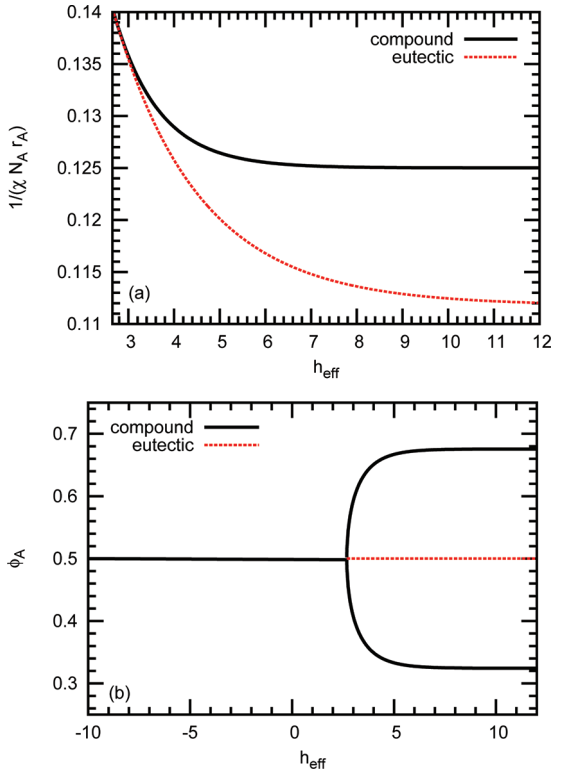

Figure 4. Comparison of the compound and eutectic (a) temperatures and (b) compositions in the spinodal for $r_A = r_B = 3$ arm A and B type monomeric units.

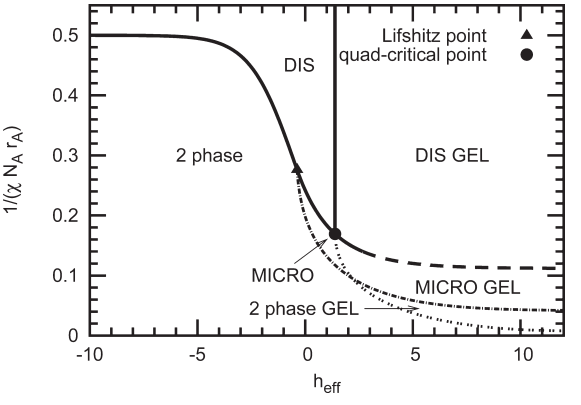

Figure 5. Mean-field phase diagram on the $z_A/z_B = 1$ isopleth for $r_A = r_B = 3$ arm A and B type monomeric units in $(\chi N_A r_A)^{-1}$ versus h_{eff} coordinates. Labeled phases are DIS (homogeneous disordered), DIS GEL (homogeneous disordered gel), 2 phase (coexisting A-rich and B-rich homogeneous phases), 2 phase GEL (coexisting A-rich and B-rich homogeneous gel phases), MICRO (microphases), and MICRO GEL (gel microphases). For values of h_{eff} higher than that at which eutectic behavior first occurs, the spinodal may not be identical to the binodal, and is indicated by the dashed curve. Hypothetical paths for the remaining boundaries, the determination of which requires full spatial calculations, are indicated by curves with double hatch marks for the boundary separating the gel from nongel regions and alternating hatch and dash marks for the boundary separating the microphase regions from coexisting homogeneous 2 phase regions.

propose hypothetical phase boundaries that require full spatial calculations (i.e., full numerical self-consistent field theory

dx.doi.org/10.1021/ma201551c |*Macromolecules* 2011, 44, 9411–9423

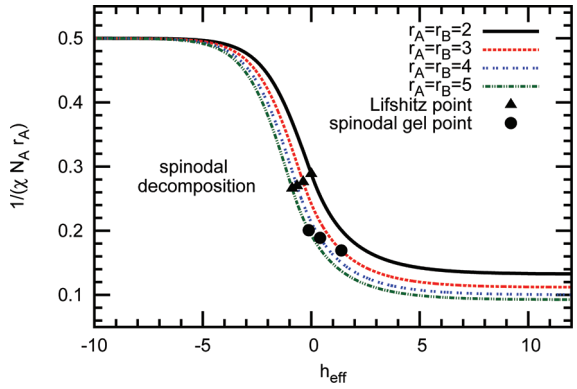

Figure 6. Spinodals in $(\chi N_A r_A)^{-1}$ versus h_{eff} coordinates indicating the limit of stability with coexisting homogeneous 2 phase regions, wavenumber $k^* = 0$, at low bond strengths, and microphases, wavenumber $k^* > 0$, at high bond strengths separated by isotropic Lifshitz points for $2 \leq r_A = r_B \leq 5$ arm A and B type monomer units. The gelation points along the spinodals for $r_A = r_B \geq 3$ are indicated on the curves. The gelation points occur along the $k^* > 0$ parts of the boundaries.

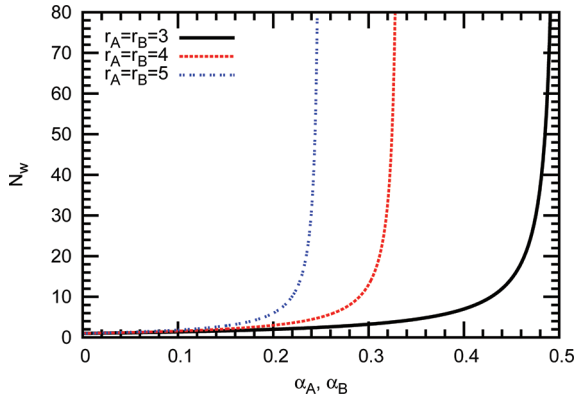

Figure 7. N_w vs α_A, α_B in the homogeneous phase for $3 \leq r_A = r_B \leq 5$ at $\phi_A = 0.5$. α_A and α_B increase with h_{eff}. $N_w \rightarrow \infty$ indicates gelation. The critical values of the fraction of A and B functional ends reacted at which gelation first occurs are given by $\alpha_{A,c} = 1/(r_A - 1)$ and $\alpha_{B,c} = 1/(r_B - 1)$, respectively.

solutions). The Lifshitz point indicates a tricritical point where the homogeneous disordered, microphase separated, and homogeneous 2 phase regions coexist. The quad-critical point corresponds to the coexistence nongel homogeneous disordered, gel homogeneous disordered, nongel microphase, and gel microphase regions.

We propose that the boundary separating the homogeneous coexisting 2 phase region from the microphases, denoted by an alternating dash and hatch mark curve, tends toward higher values of h_{eff} with lower values of temperature. This prediction is based on the work of Feng et al.[33] on the phase behavior supramolecular diblock melts, and is due to the energetic forces driving separation being dominant at low temperatures over entropic forces from the connectivity. The boundary separating the gel phases from the nongel phases, denoted by a double hatch mark curve, is also proposed to tend toward higher values of h_{eff} with lower values of temperature because as coexisting homogeneous phases become more pure with lower temperature the formation of a gel becomes less likely. The formation of a homogeneous coexisting 2 phase gel from a microphase separated

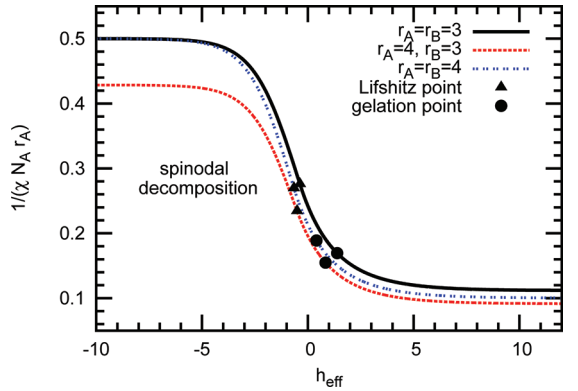

Figure 8. Spinodals in $(\chi N_A r_A)^{-1}$ versus h_{eff} coordinates indicating the limit of stability with coexisting homogeneous 2 phase regions, wavenumber $k^* = 0$, at low bond strengths, and microphases, wavenumber $k^* > 0$, at high bond strengths separated by isotropic Lifshitz points for $r_A = r_B = 3$, $r_A = 4$ and $r_B = 3$, and $r_A = r_B = 4$ arm A and B monomeric units at stoichiometric ratios of $\phi_A = 0.5$. The gelation points for disordered phases on the spinodals are indicated. The gelation points occur along the $k^* > 0$ boundaries.

gel is possible when lowering the temperature due to the reversible nature of the bonds.

The spinodals on the $z_A/z_B = 1$ isopleth were computed for $2 \leq r_A = r_B \leq 5$ arm A and B monomeric units as a function of h_{eff}. Figure 6 shows the spinodals in coordinates of $(\chi N_A r_A)^{-1}$ versus h_{eff}. The higher connectivity associated with higher functionality and higher bond strength h_{eff} shrinks the region where phase separation takes place spontaneously via spinodal decomposition. An isotropic Lifshitz point occurs at the intersection of the limit of stability with coexisting homogeneous 2 phase regions, wavenumber $k^* = 0$, at low bond strengths, and microphases, wavenumber $k^* > 0$, at high bond strengths. This indicates that at high bond strengths, separation into homogeneous A-rich and B-rich regions becomes harder due to the interconnectedness of the network, and microphase separation needs to take place. The gelation points for disordered phases on the spinodals for $r_A = r_B \geq 3$ are indicated on the curves. The gelation points occur along the $k^* > 0$ parts of the boundaries.

Gelation is indicated by the divergence of the weight-average molecular weight, N_w. Figure 7 depicts N_w versus α_A and α_B, where α_A and α_B increase with h_{eff}. The plots show that gelation in the disordered phase occurs at the values $\alpha_{A,c} = 1/(r_A - 1)$ and $\alpha_{B,c} = 1/(r_B - 1)$ for $r_A = r_B$ arm A and B monomeric units, analogous to the predictions of Flory–Stockmayer theory for a single component system. The values of bond strength corresponding to $\alpha_{A,c}$ and $\alpha_{B,c}$ in the homogeneous disordered phase are $h_{eff} = 1.386$ for $r_A = r_B = 3$, $h_{eff} = 0.405$ for $r_A = r_B = 4$, and $h_{eff} = -0.118$ for $r_A = r_B = 5$. The analogy with Flory–Stockmayer theory is expected, due to the symmetry between the A and B monomeric units in a binary disordered system with $r_A = r_B$, and due to the A and B functional ends being in stoichiometric ratio.

The critical fractional conversions $\alpha_{A,c}$ and $\alpha_{B,c}$ are related to the composition of the system through eq 37. For a system with $r_A = 3$ and $r_B = 2$ in the homogeneous phase at the stoichiometric composition of $\phi_A = 0.5$, the gelation point was found to occur at $\alpha_{A,c} = \alpha_{B,c} = 0.707$. For a system with $r_A = 4$ and $r_B = 3$ with the components in stoichiometric ratio, gelation was found to occur at $\alpha_{A,c} = \alpha_{B,c} = 0.408$. For these systems, $\alpha_{A,c} = \alpha_{B,c}$, which forces the gelation point to be such that $1/(r_A - 1) \leq \alpha_{A,c} = \alpha_{B,c} \leq 1/(r_B - 1)$.

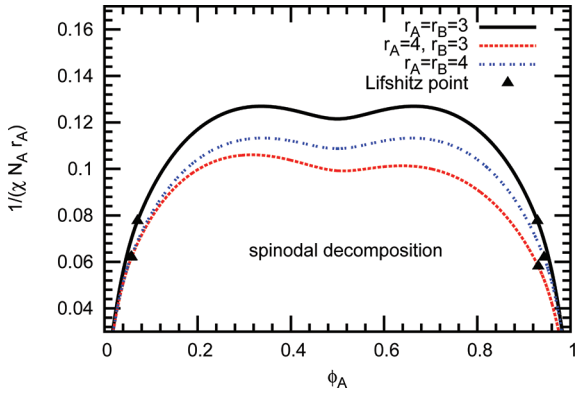

Figure 9. Spinodals in $(\chi N_A r_A)^{-1}$ versus ϕ_A coordinates indicating the limit of stability with coexisting homogeneous 2 phase regions, wavenumber $k^* = 0$, at low $(\chi N_A r_A)^{-1}$, and microphases, wavenumber $k^* > 0$, at high $(\chi N_A r_A)^{-1}$ separated by Lifshitz points for $h_{eff} = 7 - \ln 10$ with $r_A = r_B = 3$, $r_A = 4$ and $r_B = 3$, and $r_A = r_B = 4$.

The numerical solutions obtained are consistent with the theoretically predicted values of eq 35 and eq 36.

Figure 8 explores the effect of having A and B monomeric units with unequal number of arms $(r_A \neq r_B)$ on phase behavior. The phase behavior of a polymer network with A and B monomeric units with functionalities $r_A = 4$ and $r_B = 3$ is compared to the phase behavior of systems with A and B monomeric units of equal functionalities, $r_A = r_B = 3$ and $r_A = r_B = 4$, with all the polymer systems at a stoichiometric composition of $\phi_A = 0.5$. The plot of the spinodals in the $(\chi N_A r_A)^{-1}$ versus h_{eff} coordinates shows the shrinking of the regime where spinodal decomposition occurs for the $r_A = 4$, $r_B = 3$ system due to the asymmetry in the number of A and B segments. This behavior is predicted by Flory–Huggins theory in a nonbonding system. The spinodal for the $r_A = 4$, $r_B = 3$ system indicates that $(\chi N_A r_A)^{-1} = 0.429$ in the limit $h_{eff} \rightarrow -\infty$, which is lower than the value $(\chi N_A r_A)^{-1} = 0.5$ predicted for the symmetric systems. As the connectivity increases, the spinodals for the symmetric and asymmetric systems become close and parallel as $h_{eff} \rightarrow \infty$. This behavior is attributed to the connectivity playing an increasingly dominant role as the bond strength increases. The gelation points for disordered phases on the spinodals are indicated. The gelation points occur along the $k^* > 0$ boundaries.

Figure 9 depicts the spinodals in $(\chi N_A r_A)^{-1}$ versus ϕ_A coordinates for the polymer systems in Figure 8 at $h_{eff} = 7 - \ln 10$. Both the symmetric $(r_A = r_B)$ and asymmetric $(r_A \neq r_B)$ systems show eutectic behavior. The eutectic point for the asymmetric system occurs at $\phi_A = 0.512$. In the limit $h_{eff} \rightarrow \infty$, the eutectic point occurs at the stoichiometric composition $\phi_A = 0.5$. Unlike in the symmetric case, the compounds in the asymmetric system correspond to two different values of $(\chi N_A r_A)^{-1}$, and occur at $\phi_A = 0.316$ and $\phi_A = 0.638$. The compound corresponding to larger $(\chi N_A r_A)^{-1}$ occurs at $\phi_A < 0.5$ because, at these nonstoichiometric compositions, the B monomeric unit, having lower functionality, is in excess. Phase separation is more favorable for the smaller B monomeric units than for the larger A monomeric units.

4. DISCUSSION

In the present work, the field-theoretic model of Mohan et al.[26] for single-component reversibly bonding multifunctional monomeric units is extended to binary reversibly bonding multifunctional monomeric units. Following the approach of Mohan et al.,[26] the relation developed by Gordon and co-workers[17−20] between the reaction equilibria and the symmetry numbers of the polymers, where the latter are computed via the enumeration of trees formed from the graphical representation of the polymers, is embedded in a field-theoretic model. Ring formation via intramolecular reactions is not accounted for in the present framework. Intermolecular reactions are expected to be dominant in the dense melt systems considered here. Although the field-theoretic model is more generally applicable, the present study focuses on the mean-field treatment of a dense melt system. The binodals for coexisting homogeneous phases are determined from the homogeneous limit of the mean-field equations. The spinodals for various phases are found via the random phase approximation (RPA).

Phase separation and gelation are investigated for networks resulting from the heterogeneous bonding of A and B monomeric units. The binodals and spinodals of nonbonded systems correspond to that predicted by Flory–Huggins theory. Bonding between monomeric units, particularly at high functionalities and bond strengths, impedes phase separation. At sufficiently high bond strengths, coexistence between homogeneous disordered phases, microphases and gels occur. For symmetric systems, characterized by equal number of arms and arm lengths on the monomeric units at stoichiometric ratio, the gelation points in the homogeneous phase occur at the same fractions of reacted functional ends as predicted by Flory and Stockmayer for a single-component system.[1,10] Asymmetry in the number of functional ends of A and B monomeric units suppresses phase separation, and the fraction of reacted functional ends at the gelation transition are not predicted by Flory–Stockmayer theory.

The results indicate the existence of microstructured phases. Numerical self-consistent field theory calculations are needed to fully characterize these microphases, and to determine the phase boundaries referring to coexistence regions of microphases and coexistence regions of microphases and macrophases. Potential future work also includes the determination of gel phases within these microphases.

A number of isotropic Lifshitz points have been located by our mean-field RPA analysis. It is known in other contexts[41] that such multicritical points are particularly susceptible to thermal fluctuations and are replaced by regions of bicontinuous microemulsion. A more complete study of these regions would require nonmean-field techniques, such as the field-theoretic simulation method.[42]

APPENDICES

Appendix A Theoretical Formulation. We present here the derivation of eq 6 and eq 7 from eq 2, eq 3, eq 4 and eq 5. The simplifications presented in section 2.1 are achieved by relating the symmetry numbers of a polymer cluster to the number of distinct rooted, ordered trees that can be formed from the graph of the cluster. The following expressions for the number of distinct rooted, ordered trees anchored at A nodes and B nodes, $T_{A,n_A,n_B,k}$ and $T_{B,n_A,n_B,k}$, respectively, formed from the graphical representation of a cluster of n_A A-nodes and n_B B-nodes in its kth isomeric form, follow from Theorem 2 of Gordon and Temple:[18]

$$T_{A,n_A,n_B,k} = \frac{n_A r_A![(r_A-1)!]^{n_A-1}[(r_B-1)!]^{n_B}}{|G_{n_A,n_B,k}|} \qquad (44)$$

and

$$T_{\mathrm{B},n_\mathrm{A},n_\mathrm{B},k} = \frac{n_\mathrm{B} r_\mathrm{B}![(r_\mathrm{A}-1)!]^{n_\mathrm{A}}[(r_\mathrm{B}-1)!]^{n_\mathrm{B}-1}}{|G_{n_\mathrm{A},n_\mathrm{B},k}|} \tag{45}$$

The number of distinct rooted ordered trees given by eq 44 is obtained by noting the following: the anchoring node can be picked in n_A ways. This is multiplied by the $r_\mathrm{A}!$ number of ways the edges of the root can be permuted. The edges of the remaining $(n_\mathrm{A}-1)$ A-nodes can be permuted in $(r_\mathrm{A}-1)!$ ways. The edges of n_B B-nodes can be permuted in $(r_\mathrm{B}-1)!$ ways. The number of distinct rooted, ordered trees anchored at A nodes is obtained by dividing the resulting product by the symmetry number of the cluster, $|G_{n_\mathrm{A},n_\mathrm{B},k}|$. The number of distinct rooted, ordered trees rooted on B monomers is constructed analogously.

Upon solving for $|G_{n_\mathrm{A},n_\mathrm{B},k}|$ from eq 44 or eq 45 and substituting the result into eq 5, the combinatorial entropy becomes

$$\Delta S_{\mathrm{comb},n_\mathrm{A},n_\mathrm{B},k} = k_\mathrm{B}\ln\left(\frac{r_\mathrm{A}^{n_\mathrm{A}-1} r_\mathrm{B}^{n_\mathrm{B}} T_{\mathrm{A},n_\mathrm{A},n_\mathrm{B},k}}{n_\mathrm{A}}\right) \tag{46}$$

or, equivalently

$$\Delta S_{\mathrm{comb},n_\mathrm{A},n_\mathrm{B},k} = k_\mathrm{B}\ln\left(\frac{r_\mathrm{A}^{n_\mathrm{A}} r_\mathrm{B}^{n_\mathrm{B}-1} T_{\mathrm{B},n_\mathrm{A},n_\mathrm{B},k}}{n_\mathrm{B}}\right) \tag{47}$$

Equation 46 or eq 47 are substituted in eq 3 to obtain the following equivalent expressions for the activities $z_{n_\mathrm{A},n_\mathrm{B},k}$:

$$z_{n_\mathrm{A},n_\mathrm{B},k} = z_\mathrm{A}\left(\frac{z_\mathrm{A} r_\mathrm{A}}{\rho_0}\right)^{n_\mathrm{A}-1}\left(\frac{z_\mathrm{B} r_\mathrm{B}}{\rho_0}\right)^{n_\mathrm{B}} \times \frac{T_{\mathrm{A},n_\mathrm{A},n_\mathrm{B},k}}{n_\mathrm{A}} \mathrm{e}^{-\Delta G^0_{\mathrm{AA}} l_{\mathrm{AA}}/k_\mathrm{B}T - \Delta G^0_{\mathrm{BB}} l_{\mathrm{BB}}/k_\mathrm{B}T - \Delta G^0_{\mathrm{AB}} l_{\mathrm{AB}}/k_\mathrm{B}T} \tag{48}$$

or

$$z_{n_\mathrm{A},n_\mathrm{B},k} = z_\mathrm{B}\left(\frac{z_\mathrm{A} r_\mathrm{A}}{\rho_0}\right)^{n_\mathrm{A}}\left(\frac{z_\mathrm{B} r_\mathrm{B}}{\rho_0}\right)^{n_\mathrm{B}-1} \times \frac{T_{\mathrm{B},n_\mathrm{A},n_\mathrm{B},k}}{n_\mathrm{B}} \mathrm{e}^{-\Delta G^0_{\mathrm{AA}} l_{\mathrm{AA}}/k_\mathrm{B}T - \Delta G^0_{\mathrm{BB}} l_{\mathrm{BB}}/k_\mathrm{B}T - \Delta G^0_{\mathrm{AB}} l_{\mathrm{AB}}/k_\mathrm{B}T} \tag{49}$$

Substitution of eq 48 or eq 49 in eq 2 yields eq 6 or eq 7. Since eq 6 follows analogously, we present the derivation of eq 7 below. Using eq 49, the entropic terms in the Hamiltonian arising from networks having at least one B node reduce to the following:

$$\sum_{n_\mathrm{A}=0}^{\infty}\sum_{n_\mathrm{B}=1}^{\infty}\sum_k z_{n_\mathrm{A},n_\mathrm{B},k} V Q_{n_\mathrm{A},n_\mathrm{B},k}[w_\pm] = \sum_{n_\mathrm{A}=0}^{\infty}\sum_{n_\mathrm{B}=1}^{\infty}\sum_k z_\mathrm{B} V\left(\frac{z_\mathrm{A} r_\mathrm{A}}{\rho_0}\right)^{n_\mathrm{A}}\left(\frac{z_\mathrm{B} r_\mathrm{B}}{\rho_0}\right)^{n_\mathrm{B}-1}\frac{T_{\mathrm{B},n_\mathrm{A},n_\mathrm{B},k}}{n_\mathrm{B}} \times \mathrm{e}^{-\Delta G^0_{\mathrm{AA}} l_{\mathrm{AA}}/k_\mathrm{B}T - \Delta G^0_{\mathrm{BB}} l_{\mathrm{BB}}/k_\mathrm{B}T - \Delta G^0_{\mathrm{AB}} l_{\mathrm{AB}}/k_\mathrm{B}T} Q_{n_\mathrm{A},n_\mathrm{B},k}[w_\pm] \tag{50}$$

We introduce the partition function of trees rooted on a B node as follows:

$$Q^T_{n_\mathrm{A},n_\mathrm{B},\mathrm{B}}[w_\pm] = \sum_k T_{\mathrm{B},n_\mathrm{A},n_\mathrm{B},k} Q_{n_\mathrm{A},n_\mathrm{B},k}[w_\pm] \tag{51}$$

Upon introducing the propagator to the root node of rooted, ordered trees rooted on a B node summed over all such distinct trees, $q^T_{n_\mathrm{A},n_\mathrm{B},\mathrm{B}}(\mathbf{r},[w_\pm])$, the partition function $Q^T_{n_\mathrm{A},n_\mathrm{B},\mathrm{B}}$ becomes

$$Q^T_{n_\mathrm{A},n_\mathrm{B},\mathrm{B}}[w_\pm] = \frac{1}{V}\int \mathrm{d}\mathbf{r}\, q^T_{n_\mathrm{A},n_\mathrm{B},\mathrm{B}}(\mathbf{r},[w_\pm]) \tag{52}$$

Therefore, we obtain

$$\sum_{n_\mathrm{A}=0}^{\infty}\sum_{n_\mathrm{B}=1}^{\infty}\sum_k z_{n_\mathrm{A},n_\mathrm{B},k} V Q_{n_\mathrm{A},n_\mathrm{B},k}[w_\pm] = \sum_{n_\mathrm{A}=0}^{\infty}\sum_{n_\mathrm{B}=1}^{\infty} z_\mathrm{B}\left(\frac{z_\mathrm{A} r_\mathrm{A}}{\rho_0}\right)^{n_\mathrm{A}}\left(\frac{z_\mathrm{B} r_\mathrm{B}}{\rho_0}\right)^{n_\mathrm{B}-1} \times \mathrm{e}^{-\Delta G^0_{\mathrm{AA}} l_{\mathrm{AA}}/k_\mathrm{B}T - \Delta G^0_{\mathrm{BB}} l_{\mathrm{BB}}/k_\mathrm{B}T - \Delta G^0_{\mathrm{AB}} l_{\mathrm{AB}}/k_\mathrm{B}T} \times \frac{1}{n_\mathrm{B}}\int \mathrm{d}\mathbf{r}\, q^T_{n_\mathrm{A},n_\mathrm{B},\mathrm{B}}(\mathbf{r},[w_\pm]) \tag{53}$$

The summations in eq 53 are evaluated by introducing a generating function that reproduces all conformations for trees rooted on a B node, with a weighting factor of $\exp[-\Delta G^0_{\mathrm{AA}}/(k_\mathrm{B}T)]$, $\exp[-\Delta G^0_{\mathrm{BB}}/(k_\mathrm{B}T)]$, or $\exp[-\Delta G^0_{\mathrm{AB}}/(k_\mathrm{B}T)]$, arising from the presence of A−A, B−B or A−B bonds, respectively, and with A nodes weighted by the factor $z_\mathrm{A} r_\mathrm{A}/\rho_0$, and additional B nodes apart from the root node weighted by the factor $z_\mathrm{B} r_\mathrm{B}/\rho_0$. The necessary generating function is simply constructed by inspection,[26] yielding eq 9. It is readily verified that eq 9 is represented by the following series expansion:

$$F_{0\mathrm{B}}(\mathbf{r},\theta_\mathrm{A},\theta_\mathrm{B},[w_\pm]) = \sum_{n_\mathrm{A}=0}^{\infty}\sum_{n_\mathrm{B}=1}^{\infty}\left(\frac{z_\mathrm{A} r_\mathrm{A}}{\rho_0}\right)^{n_\mathrm{A}}\left(\frac{z_\mathrm{B} r_\mathrm{B}}{\rho_0}\right)^{n_\mathrm{B}-1} \times \mathrm{e}^{-\Delta G^0_{\mathrm{AA}} l_{\mathrm{AA}}/k_\mathrm{B}T - \Delta G^0_{\mathrm{BB}} l_{\mathrm{BB}}/k_\mathrm{B}T - \Delta G^0_{\mathrm{AB}} l_{\mathrm{AB}}/k_\mathrm{B}T} \times \theta_\mathrm{A}^{n_\mathrm{A}}\theta_\mathrm{B}^{n_\mathrm{B}-1} q^T_{n_\mathrm{A},n_\mathrm{B},\mathrm{B}}(r,[w_\pm]) \tag{54}$$

where θ_A and θ_B are auxiliary variables such that the coefficient of $\theta_\mathrm{A}^{n_\mathrm{A}}\theta_\mathrm{B}^{n_\mathrm{B}-1}$ represents trees having n_A A-nodes and n_B B-nodes rooted on a B node. Consequently, eq 53 reduces to the form

$$\sum_{n_\mathrm{A}=0}^{\infty}\sum_{n_\mathrm{B}=1}^{\infty}\sum_k z_{n_\mathrm{A},n_\mathrm{B},k} V Q_{n_\mathrm{A},n_\mathrm{B},k}[w_\pm] = z_\mathrm{B}\int \mathrm{d}\mathbf{r}\int_0^1 \mathrm{d}\theta_\mathrm{B}\, F_{0\mathrm{B}}(\mathbf{r},\theta_\mathrm{A}=1,\theta_\mathrm{B},[w_\pm]) \tag{55}$$

The generating function $F_{0\mathrm{A}}$ for the conformation of trees rooted on A nodes, given by eq 8, is obtained analogously and possesses the series expansion

$$F_{0\mathrm{A}}(r,\theta_\mathrm{A},\theta_\mathrm{B},[w_\pm]) = \sum_{n_\mathrm{A}=1}^{\infty}\sum_{n_\mathrm{B}=0}^{\infty}\left(\frac{z_\mathrm{A} r_\mathrm{A}}{\rho_0}\right)^{n_\mathrm{A}-1}\left(\frac{z_\mathrm{B} r_\mathrm{B}}{\rho_0}\right)^{n_\mathrm{B}} \times \mathrm{e}^{-\Delta G^0_{\mathrm{AA}} l_{\mathrm{AA}}/k_\mathrm{B}T - \Delta G^0_{\mathrm{BB}} l_{\mathrm{BB}}/k_\mathrm{B}T - \Delta G^0_{\mathrm{AB}} l_{\mathrm{AB}}/k_\mathrm{B}T} \times \theta_\mathrm{A}^{n_\mathrm{A}-1}\theta_\mathrm{B}^{n_\mathrm{B}} q^T_{n_\mathrm{A},n_\mathrm{B},\mathrm{A}}(r,[w_\pm]) \tag{56}$$

where $q^T_{n_\mathrm{A},n_\mathrm{B},\mathrm{A}}(\mathbf{r},[w_\pm])$ denotes the propagator to the root node of distinct rooted, ordered trees rooted on an A node, summed over all such trees. The coefficient of $\theta_\mathrm{A}^{n_\mathrm{A}-1}\theta_\mathrm{B}^{n_\mathrm{B}}$ represents trees having n_A A-nodes and n_B B-nodes rooted on an A node.

The entropic contribution to the Hamiltonian from trees possessing A units alone becomes

$$\sum_{n_A=1}^{\infty}\sum_{k} z_{n_A,n_B=0,k} VQ_{n_A,n_B=0,k}[w_\pm] = z_A\int \mathrm{d}\mathbf{r}\int_0^1 \mathrm{d}\theta_A\, F_{0A}(\mathbf{r},\theta_A,\theta_B=0,[w_\pm]) \quad (57)$$

Consequently, we obtain the following net entropic contribution to the Hamiltonian:

$$\sum_{n_A=0}^{\infty}\sum_{n_B=0}^{\infty}\sum_{k} z_{n_A,n_B,k} VQ_{n_A,n_B,k}[w_\pm] = z_B\int \mathrm{d}\mathbf{r}\int_0^1 \mathrm{d}\theta_B\, F_{0B}(\mathbf{r},\theta_A=1,\theta_B,[w_\pm]) + z_A\int \mathrm{d}\mathbf{r}\int_0^1 \mathrm{d}\theta_A\, F_{0A}(\mathbf{r},\theta_A,\theta_B=0,[w_\pm]) \quad (58)$$

The above formulation may be regarded as a branching process,[43] where the root unit constitutes the 0th generation and upon reaction, gives rise successively to the 1st, 2nd, ..., generations. We model the process as a multitype branching process,[43] where discretized values of the spatial variable and the chemical identities of the units (i.e., A or B) together constitute a finite number of "types."[26] Within this framework, the generating functions may be obtained both before the gel point for the sol phase, and after the gel point for both sol and gel phases. Before the gel point is reached, the smallest roots of F_{1A} and F_{1B} yield the desired statistical weights of all trees at all spatial locations. However, after gelation, the smallest roots of F_{1A} and F_{1B} yield the desired statistical weights only for finite trees in the sol phase. The next larger roots of F_{1A} and F_{1B} yield the statistical weights of all finite and infinite trees, and are used to compute total densities and conversions.[26,43]

Appendix B RPA. The weak inhomogeneous field expansion of the fields given by eq 38 results in

$$F_{1J}(\bar{\mathbf{k}}) = F_{1J}^{(0)} + F_{1J}^{(1)}(\bar{\mathbf{k}}) \quad (59)$$

for the generating functions F_{1A} and F_{1B}. The $\mathcal{O}(1)$ coefficients of the generating function expansions are

$$F_{1A}^{(0)} = \left(q_{0A}^{(0)}(1) + \frac{\bar{z}_B r_B}{N_A}\mathrm{e}^{-\Delta G_{AB}^0/k_BT}\theta_B G_A^{(0)}(0,1)G_B^{(0)}(0,f_B)F_{1B}^{(0)}\right)^{r_A-1} \quad (60)$$

and

$$F_{1B}^{(0)} = \left(q_{0B}^{(0)}(f_B) + \frac{\bar{z}_A r_A}{N_A}\mathrm{e}^{-\Delta G_{AB}^0/k_BT}\theta_A G_B^{(0)}(0,f_B)G_A^{(0)}(0,1)F_{1A}^{(0)}\right)^{r_B-1} \quad (61)$$

and the $\mathcal{O}(\varepsilon)$ coefficients of the generating function expansions are

$$F_{1A}^{(1)}(\bar{\mathbf{k}}) = (r_A-1)F_{1A}^{(0)[(r_A-2)/(r_A-1)]}\times\left(q_{0A}^{(1)}(\bar{\mathbf{k}},1) + \frac{\bar{z}_B r_B}{N_A}\mathrm{e}^{-\Delta G_{AB}^0/k_BT}\theta_B(G_A^{(1)}(\bar{\mathbf{k}},0,1)G_B^{(0)} \times(0,f_B)F_{1B}^{(0)} + G_A^{(0)}(\bar{\mathbf{k}},1)G_B^{(1)}(\bar{\mathbf{k}},0,f_B)F_{1B}^{(0)} + G_A^{(0)}(\bar{\mathbf{k}},1)G_B^{(0)}(\bar{\mathbf{k}},f_B)F_{1B}^{(1)}(\bar{\mathbf{k}}))\right) \quad (62)$$

and

$$F_{1B}^{(1)}(\bar{\mathbf{k}}) = (r_B-1)F_{1B}^{(0)[(r_B-2)/(r_B-1)]}\times\left(q_{0B}^{(1)}(\bar{\mathbf{k}},f_B) + \frac{\bar{z}_A r_A}{N_A}\mathrm{e}^{-\Delta G_{AB}^0/k_BT}\theta_A(G_B^{(1)}(\bar{\mathbf{k}},0,f_B)G_A^{(0)}(0,1)F_{1A}^{(0)} + G_B^{(0)}(\bar{\mathbf{k}},f_B)G_A^{(1)}(\bar{\mathbf{k}},0,1)F_{1A}^{(0)} + G_B^{(0)}(\bar{\mathbf{k}},f_B)G_A^{(0)}(\bar{\mathbf{k}},1)F_{1A}^{(1)}(\bar{\mathbf{k}}))\right) \quad (63)$$

where $G_J^{(0)}(\bar{\mathbf{k}},\bar{s})$ are the $\mathcal{O}(1)$ coefficients and $G_J^{(1)}(\bar{\mathbf{k}},\bar{\mathbf{k}}',\bar{s})$ are the $\mathcal{O}(\varepsilon)$ coefficients of the Green's function expansion in powers of ε. The Green's function expansion coefficients are[36]

$$G_J^{(0)}(\bar{\mathbf{k}},\bar{s}) = \mathrm{e}^{-\bar{s}\bar{k}^2 - \bar{w}_{J0}\bar{s}} \quad (64)$$

and

$$G_J^{(1)}(\bar{\mathbf{k}},\bar{\mathbf{k}}',\bar{s}) = \mathrm{e}^{-\bar{w}_{J0}\bar{s}}\frac{\mathrm{e}^{-\bar{s}\bar{k}^2} - \mathrm{e}^{-\bar{s}\bar{k}'^2}}{\bar{k}^2-\bar{k}'^2}\omega_J(\bar{\mathbf{k}}) \quad (65)$$

The $\mathcal{O}(1)$ and $\mathcal{O}(\varepsilon)$ coefficients for the free chain propagators, respectively, obtained from eq 13 are

$$q_{0J}^{(0)}(\bar{s}) = \mathrm{e}^{-\bar{w}_{J0}\bar{s}} \quad (66)$$

and

$$q_{0J}^{(1)}(\bar{\mathbf{k}},\bar{s}) = -\omega_J(\bar{\mathbf{k}})\mathrm{e}^{-\bar{w}_{J0}\bar{s}}\frac{1-\mathrm{e}^{-\bar{s}\bar{k}^2}}{\bar{k}^2} \quad (67)$$

The $\mathcal{O}(1)$ coefficients of the volume fractions in eq 40 are given by

$$\phi_A^{(0)} = \bar{z}_A r_A\int_0^1 \mathrm{d}\bar{s}\left(G_A^{(0)}(0,1-\bar{s})F_{1A}^{(0)} \times\left(G_A^{(0)}(0,\bar{s}) + \frac{\bar{z}_B r_B}{N_A}\mathrm{e}^{-\Delta G_{AB}^0/k_BT}G_A^{(0)}(0,\bar{s})G_B^{(0)}(0,f_B)F_{1B}^{(0)}\right)\right) \quad (68)$$

and

$$\phi_B^{(0)} = \bar{z}_B r_B\int_0^{f_B} \mathrm{d}\bar{s}\left(G_B^{(0)}(0,f_B-\bar{s})F_{1B}^{(0)} \times\left(G_B^{(0)}(0,\bar{s}) + \frac{\bar{z}_A r_A}{N_A}\mathrm{e}^{-\Delta G_{AB}^0/k_BT}G_B^{(0)}(0,\bar{s})G_A^{(0)}(0,1)F_{1A}^{(0)}\right)\right) \quad (69)$$

and the $\mathcal{O}(\varepsilon)$ coefficients of the volume fractions are

$$\delta\phi_A(\bar{\mathbf{k}}) = \bar{z}_A r_A\int_0^1 \mathrm{d}\bar{s}\left(G_A^{(0)}(0,1-\bar{s})F_{1A}^{(0)} \times\left(G_A^{(1)}(\bar{\mathbf{k}},0,\bar{s}) + \frac{\bar{z}_B r_B}{N_A}\mathrm{e}^{-\Delta G_{AB}^0/k_BT}(G_A^{(1)}(\bar{\mathbf{k}},0,\bar{s})G_B^{(0)}(0,f_B)F_{1B}^{(0)} + G_A^{(0)}(\bar{\mathbf{k}},\bar{s})G_B^{(1)}(\bar{\mathbf{k}},0,f_B)F_{1B}^{(0)} + G_A^{(0)}(\bar{\mathbf{k}},\bar{s})G_B^{(0)}(\bar{\mathbf{k}},f_B)F_{1B}^{(1)}(\bar{\mathbf{k}}))\right) + (G_A^{(1)}(\bar{\mathbf{k}},0,1-\bar{s})F_{1A}^{(0)} + G_A^{(0)}(\bar{\mathbf{k}},1-\bar{s})F_{1A}^{(1)}(\bar{\mathbf{k}})) \times\left(G_A^{(0)}(0,\bar{s}) + \frac{\bar{z}_B r_B}{N_A}\mathrm{e}^{-\Delta G_{AB}^0/k_BT}G_A^{(0)}(0,\bar{s})G_B^{(0)}(0,f_B)F_{1B}^{(0)}\right)\right) \quad (70)$$

and

$$\delta\phi_B(\bar{k}) = \bar{z}_B r_B \int_0^{f_B} d\bar{s} \Bigg(G_B^{(0)}(0, f_B - \bar{s}) F_{1B}^{(0)} \times \Bigg(G_B^{(1)}(\bar{k}, 0, \bar{s}) + \frac{\bar{z}_A r_A}{N_A} e^{-\Delta G_{AB}^0/k_B T} (G_B^{(1)}(\bar{k}, 0, \bar{s}) G_A^{(0)}(0, 1) F_{1A}^{(0)} + G_B^{(0)}(\bar{k}, \bar{s}) G_A^{(1)}(\bar{k}, 0, 1) F_{1A}^{(0)} + G_B^{(0)}(\bar{k}, \bar{s}) G_A^{(0)}(\bar{k}, 1) F_{1A}^{(1)}(\bar{k})) \Bigg) + (G_B^{(1)}(\bar{k}, 0, f_B - \bar{s}) F_{1B}^{(0)} + G_B^{(0)}(\bar{k}, f_B - \bar{s}) F_{1B}^{(1)}(\bar{k})) \times \Bigg(G_B^{(0)}(0, \bar{s}) + \frac{\bar{z}_A r_A}{N_A} e^{-\Delta G_{AB}^0/k_B T} G_B^{(0)}(0, \bar{s}) G_A^{(0)}(0, 1) F_{1A}^{(0)} \Bigg) \Bigg) \tag{71}$$

The $\mathcal{O}(\varepsilon)$ expansions of the volume fractions given by eq 70 and eq 71 written in the form of eq 41 and eq 42 results in the density−density correlation functions in Fourier space for Gaussian chains in the absence of external fields, $S_{AA}(\bar{k})$, $S_{AB}(\bar{k})$, and $S_{BB}(\bar{k})$.

Appendix C Gelation Condition. In the special case of a homogeneous system, the functions $F_{1A}^{(0)}$ and $F_{1B}^{(0)}$, where the superscript "(0)" indicates the homogeneous solution, may be simplified by employing the homogeneous Green's functions presented in Appendix B. For the special case where only heterogeneous bonding between A and B units occurs, we obtain

$$F_{1A}^{(0)} = e^{-\bar{w}_{A0}(r_A - 1)} \left(1 + \frac{\bar{z}_B r_B}{N_A} e^{-\Delta G_{AB}^0/k_B T} e^{-\bar{w}_{B0} N_B/N_A} \theta_B F_{1B}^{(0)} \right)^{r_A - 1} \tag{72}$$

and

$$F_{1B}^{(0)} = e^{-(\bar{w}_{B0} N_B/N_A)(r_B - 1)} \left(1 + \frac{\bar{z}_A r_A}{N_A} e^{-\Delta G_{AB}^0/k_B T} e^{-\bar{w}_{A0}} \theta_A F_{1A}^{(0)} \right)^{r_B - 1} \tag{73}$$

Furthermore, the fractional conversions α_A and α_B reduce to the following expressions for a heterogeneously-bonded, spatially homogeneous system:

$$\alpha_A = \frac{\frac{\bar{z}_B r_B}{N_A} e^{-\Delta G_{AB}^0/k_B T} e^{-\bar{w}_{B0} N_B/N_A} F_{1B}^{(0)}}{1 + \frac{\bar{z}_B r_B}{N_A} e^{-\Delta G_{AB}^0/k_B T} e^{-\bar{w}_{B0} N_B/N_A} F_{1B}^{(0)}} \tag{74}$$

and

$$\alpha_B = \frac{\frac{\bar{z}_A r_A}{N_A} e^{-\Delta G_{AB}^0/k_B T} e^{-\bar{w}_{A0}} F_{1A}^{(0)}}{1 + \frac{\bar{z}_A r_A}{N_A} e^{-\Delta G_{AB}^0/k_B T} e^{-\bar{w}_{A0}} F_{1A}^{(0)}} \tag{75}$$

Upon combining eq 74 and eq 75 with eq 72 and eq 73 at $\theta_A = \theta_B = 1$, we obtain

$$F_{1A}^{(0)}(\theta_A = 1, \theta_B = 1) = \left(\frac{e^{-\bar{w}_{A0}}}{1 - \alpha_A} \right)^{r_A - 1} \tag{76}$$

and

$$F_{1B}^{(0)}(\theta_A = 1, \theta_B = 1) = \left(\frac{e^{-\bar{w}_{B0} N_B/N_A}}{1 - \alpha_B} \right)^{r_B - 1} \tag{77}$$

We now introduce the normalized generating functions $\tilde{F}_{1A}^{(0)}(\theta_A,\theta_B) = F_{1A}^{(0)}(\theta_A,\theta_B)/F_{1A}^{(0)}(\theta_A = 1,\theta_B = 1)$ and $\tilde{F}_{1B}^{(0)}(\theta_A,\theta_B) = F_{1B}^{(0)}(\theta_A,\theta_B)/F_{1B}^{(0)}(\theta_A = 1,\theta_B = 1)$, which may be expressed in terms of the homogeneous fractional conversions α_A and α_B upon simplification as follows:

$$\tilde{F}_{1A}^{(0)} = (1 - \alpha_A + \alpha_A \theta_B \tilde{F}_{1B}^{(0)})^{r_A - 1} \tag{78}$$

and

$$\tilde{F}_{1B}^{(0)} = (1 - \alpha_B + \alpha_B \theta_A \tilde{F}_{1A}^{(0)})^{r_B - 1} \tag{79}$$

The generating functions may be expressed in the form of infinite iterates, $u_A = \theta_A \tilde{F}_{1A}^{(0)}(u_B)$ and $u_B = \theta_B \tilde{F}_{1B}^{(0)}(u_A)$, corresponding to the probability generating functions[24,25,43] for the first (and subsequent) generation subtrees rooted on A and B units, respectively, such that the coefficients of $\theta_A^{n_A}\theta_B^{n_B}$ yield the probabilities of having subtrees of n_A A units and n_B B units rooted on A and B units, respectively. These functions are equivalent to the recurrence relations given by eq 72 and eq 73, subject to a normalization factor. In addition, the probability generating functions for the number of children of types A or B, for a root unit of type A or B in the first generation,[24,25,43] are given by the equations

$$\tilde{F}_{1A}^{(0)}(u_B) = (1 - \alpha_A + \alpha_A u_B)^{r_A - 1} \tag{80}$$

and

$$\tilde{F}_{1B}^{(0)}(u_A) = (1 - \alpha_B + \alpha_B u_A)^{r_B - 1} \tag{81}$$

respectively, in the dummy variables u_A and u_B. These probability generating functions may also be constructed directly from probabilistic arguments. Gelation occurs when the extinction probabilities[43] for the process starting from an A or a B unit fall below unity, indicating the formation of an infinite tree structure. The following condition must be satisfied for the formation of an infinite tree structure:[24,43]

$$\begin{vmatrix} \left[\frac{\partial \tilde{F}_{1A}^{(0)}}{\partial u_A}\right]_{u_A = u_B = 1} - 1 & \left[\frac{\partial \tilde{F}_{1A}^{(0)}}{\partial u_B}\right]_{u_A = u_B = 1} \\ \left[\frac{\partial \tilde{F}_{1B}^{(0)}}{\partial u_A}\right]_{u_A = u_B = 1} & \left[\frac{\partial \tilde{F}_{1B}^{(0)}}{\partial u_B}\right]_{u_A = u_B = 1} - 1 \end{vmatrix} = 0 \tag{82}$$

Substitution of eq 80 and eq 81 in eq 82 finally yields

$$\alpha_{A,c}\alpha_{B,c} = \frac{1}{(r_A - 1)(r_B - 1)} \tag{83}$$

where the subscript "c" refers to the critical fractional conversions at the gel point.

In a homogeneous system, by definition, the end segment volume fractions and total volume fractions, respectively, are

$$\phi_{J,e} = \frac{n_J r_J}{n_A r_A N_A + n_B N_B r_B} \tag{84}$$

and

$$\phi_J = \frac{n_J r_J N_J}{n_A r_A N_A + n_B N_B r_B} \tag{85}$$

where $J = \{A,B\}$. In a heterogeneously-bonding system, A and B monomeric units must have the same number of reacted end segments. This results in the following relation between the

fractions of reacted A and B functional ends for a homogeneous system:

$$\frac{\alpha_A}{\alpha_B} = \frac{N_A \phi_B}{N_B \phi_A} \tag{86}$$

Upon combining eq 83 with eq 86, we obtain the following expressions for the critical fractional conversions in a heterogeneously-bonded system:

$$\alpha_{A,c} = \sqrt{\frac{\phi_B N_A}{\phi_A N_B (r_A - 1)(r_B - 1)}} \tag{87}$$

and

$$\alpha_{B,c} = \sqrt{\frac{\phi_A N_B}{\phi_B N_A (r_A - 1)(r_B - 1)}} \tag{88}$$

where the subscript "c" refers to the critical fractional conversions at the gel point.

AUTHOR INFORMATION

Corresponding Author

*E-mail: ghf@mrl.ucsb.edu.

ACKNOWLEDGMENT

This work was supported by NSF Grant No. DMR09-04499 and a grant from the DSM Corporation, and made use of MRL Central Facilities supported by the MRSEC Program of the NSF under Grant No. DMR05-20415. Mester would like to acknowledge the California NanoSystems Institute for its support through a graduate fellowship.

REFERENCES

(1) Flory, P. J. *Principles of Polymer Chemistry*; Cornell University Press: Ithaca, NY, 1953.
(2) Tang, C.; Lennon, E. M.; Fredrickson, G. H.; Kramer, E. J.; Hawker, C. J. *Science* **2008**, *322*, 429–432.
(3) Beck, J. B.; Rowan, S. J. *J. Am. Chem. Soc.* **2003**, *125*, 13922.
(4) Lange, R. F. M.; van Gurp, M.; Meijer, E. W. *J. Polym. Sci.: Part A: Polym. Chem.* **1999**, *37*, 3657–3670.
(5) Kihara, H.; Kato, T.; Uryu, T.; Frechet, J. M. J. *Chem. Mater.* **1996**, *8*, 961–968.
(6) Chino, K.; Ashiura, M. *Macromolecules* **2001**, *34*, 9201–9204.
(7) Cordier, P.; Tournilhac, F.; Soulie-Ziakovic, C.; Leibler, L. *Nature* **2008**, *46*, 977–980.
(8) Skrzeszewska, P. J.; Sprakel, J.; de Wolf, F. A.; Fokkink, R.; Stuart, M. A. C.; van der Gucht, J. *Macromolecules* **2010**, *43*, 3542–3548.
(9) Sijbesma, R. P.; Beijer, F. H.; Brunsveld, L.; Folmer, B. J. B.; Hirschberg, J. H. K. K.; Lange, R. F. M.; Lowe, J. K. L.; Meijer, E. W. *Science* **1997**, *28*, 1601–1604.
(10) Stockmayer, W. H. *J. Chem. Phys.* **1943**, *11*, 45–55.
(11) Coniglio, A.; Stanley, H. E.; Klein, W. *Phys. Rev. Lett.* **1979**, *42*, 518–522.
(12) Coniglio, A.; Stanley, H. E.; Klein, W. *Phys. Rev. B* **1982**, *25*, 6805–6821.
(13) Fierro, A.; del Gado, E.; de Candia, A.; Coniglio, A. *J. Stat. Mech.* **2008**, L04002.
(14) Sator, N. *Phys. Rep.* **2003**, *376*, 1–39.
(15) Hoy, R. S.; Fredrickson, G. H. *J. Chem. Phys.* **2009**, *131*, 224902.
(16) Rubinstein, M.; Dobrynin, A. V. *Curr. Opin. Colloid Interface Sci.* **1999**, *4*, 83.
(17) Gordon, M.; Judd, M. *Nature* **1971**, *234*, 96–97.
(18) Gordon, M.; Temple, W. B. *J. Chem. Soc. A* **1970**, 729–737.
(19) Gordon, M.; Scantlebury, G. R. *Trans. Faraday Soc* **1964**, *60*, 604–621.
(20) Gordon, M.; Temple, W. B. In *Chemical Applications of Graph Theory*; Balaban, A. T., Ed.; Academic Press: London, 1976.
(21) Dobson, G. R.; Gordon, M. *J. Chem. Phys.* **1964**, *41*, 2389.
(22) Gordon, M.; Malcolm, G. N. *Proc. R. Soc. London A* **1966**, *295*, 29.
(23) Dobson, G. R.; Gordon, M. *J. Chem. Phys.* **1965**, *43*, 705.
(24) Gordon, M. *Proc. R. Soc. London, Ser. A* **1962**, *268*, 240–256.
(25) Good, I. J. *Proc. R. Soc. London, Ser. A* **1963**, *272*, 54–59.
(26) Mohan, A.; Elliot, R.; Fredrickson, G. H. *J. Chem. Phys.* **2010**, *133*, 174903.
(27) Leibler, L. *Macromolecules* **1980**, *13*, 1602–1617.
(28) Matsen, M. W.; Schick, M. *Phys. Rev. Lett.* **1994**, *72*, 2660–2663.
(29) Matsen, M. W.; Bates, F. S. *Macromolecules* **1996**, *29*, 1091–1098.
(30) Matsen, M. W. *Macromolecules* **1995**, *28*, 5765–5773.
(31) Matsen, M. W. *Phys. Rev. Lett.* **1995**, *74*, 4225–4228.
(32) Bates, F. S.; Maurer, W.; Lodge, T. P.; Schulz, M. F.; Matsen, M. W.; Almdal, K.; Mortensen, K. *Phys. Rev. Lett.* **1995**, *75*, 4429–4432.
(33) Feng, E. H.; Lee, W. B.; Fredrickson, G. H. *Macromolecules* **2007**, *40*, 693–702.
(34) Lee, W. B.; Elliott, R.; Katsov, K.; Fredrickson, G. H. *Macromolecules* **2007**, *40*, 8445–8454.
(35) Elliott, R.; Fredrickson, G. H. *J. Chem. Phys.* **2009**, *131*, 144906.
(36) Fredrickson, G. H. *The Equilibrium Theory of Inhomogeneous Polymers*; Oxford Science Publications: Oxford, 2006.
(37) McQuarrie, D. A. *Statistical Mechanics*; University Science Books: Sausalito, CA, 2000.
(38) Rosen, K. H.; Michaels, J. G.; Gross, J. L.; Grossman, J. W.; Shier, D. R. *Handbook of Discrete and Combinatorial Mathematics*; CRC Press: Boca Raton, FL, 2000.
(39) Harary, F. *Graph Theory*; Addison-Wesley: Reading, MA, 1969.
(40) Press, W. H.; Teukolsky, S. A.; Vetterling, W. T.; Flannery, B. P. *Numerical Recipes in C++: The Art of Scientific Computing*, 2nd ed.; Cambridge University Press: New York, 2003.
(41) Bates, F. S.; Maurer, W. W.; Lipic, P. M.; Hillmyer, M. A.; Almdal, K.; Mortensen, K.; Fredrickson, G. H.; Lodge, T. P. *Phys. Rev. Lett.* **1997**, *79*, 849–852.
(42) Duechs, D.; Ganesan, V.; Fredrickson, G. H. *Macromolecules* **2003**, *36*, 9237–9248.
(43) Harris, T. E. *The Theory of Branching Processes*; Springer-Verlag: Berlin, 1963.